ChemComm

COMMUNICATION

View Article Online
View Journal

Cite this: DOI: 10.1039/d1cc05629h

Received 6th October 2021,
Accepted 6th December 2021

DOI: 10.1039/d1cc05629h

rsc.li/chemcomm

Spatially isolated CoN_x quantum dots on carbon nanotubes enable a robust radical-free Fenton-like process†

Jia-Cheng E. Yang, [a] Min-Ping Zhu,[ab] Darren Delai Sun, [c] Ming-Lai Fu *[ad] and Yu-Ming Zheng *[ab]

We unprecedentedly report spatially separated CoN_x nanodots on carbon nanotubes (CNTs) *via* a facile formamide condensation reaction. To our knowledge, CoN_x-CNTs outperform the activities of current catalysts in peroxymonosulfate activation. CoN_x-CNT-oriented radical-free degradation of contaminants shows robust anti-interference capacity toward environmental conditions. Our work will stimulate general interest in designing cost-effective and versatile quantum-/atom-sized catalysts with fully exposed active sites for water purification and beyond.

The generation of reactive species is of vital importance to environmental remediation, biogeochemical cycle, photodynamic therapy and energy exploration.[1–7] Among all the reactive species, the hydrogen radical ($^{\bullet}OH$, 1.9–2.7 V_{NHE}) and sulfate radical ($SO_4^{\bullet-}$, 2.6–3.1 V_{NHE}) have long been considered as one of the strongest oxidants to degrade a wide array of refractory organic contaminants (ROCs) because of their oxidation potential;[8,9] however, their high reactivities for both the target pollutants and the competing environmental constituents in wastewaters can cause undesirable performance for water detoxication.[10,11] Meanwhile, radical-free oxidants, such as $^1O_2$, peroxy–metal complexes and high-valence metal-oxo species, have recently attracted significant attention due to their intrinsic and robust anti-interference capacity toward diverse scavengers, anions and natural organic matter.[12–14] Therefore, there has been a gradual paradigm shift in strategies for degrading ROCs from a free radical process to a radical-free pathway.[15,16]

Manipulating the structure/properties of materials at the atom- and/or quantum-sized scale has been suggested as an effective strategy to fully expose their active sites with a theoretical 100% atom utilization rate, allowing control of the formation of reactive species.[17–20] The basic understanding shows that the formation of radical-free oxidants is highly reliant on a few factors such as exposed catalytically active sites, active site geometry and the size of the active site itself.[21–23] For instance, recently reported single-atom catalysts with CoN_{2+2} and FeN_4 configurations on carbon supports exhibited a high selectivity of activating/catalysing peroxymonosulfate (PMS) to form $^1O_2$ without generating $^{\bullet}OH$, $SO_4^{\bullet-}$ and $O_2^{\bullet-}$.[23,24] Under nanoconfinement, H_2O_2 was catalytically decomposed into $^1O_2$ by 2 nm Fe_2O_3 quantum dots confined in the nanochannels of multi-walled carbon nanotubes (CNTs).[25] Despite the interesting and impressive results of selectively producing radical-free species, the synthesis of such tiny and sophisticated catalysts is not cost-effective and even less environmentally-friendly. The time, energy and chemically intensive procedures usually involved in the synthesis of catalysts and their precursors (refer to Table S1 (ESI†)) would become the bottlenecks of practical engineering. Thus, there is an urgent need to develop a cost-effective method to synthesize innovative catalysts with tailored structures and active site regimes for highly and selectively producing non-radical species.

Herein, we report a facile, mild and cost-effective strategy for synthesizing CoN_x nanoclusters (<15 nm) spatially isolated on the surface of CNTs. We also demonstrate a robust non-radical oxidation process realized by CoN_x-CNTs. The commercial multiwalled CNTs, FA, and $Co(NO_3)_2{\cdot}6H_2O$ can be easily self-assembled into CoN_x-CNTs *via* a simple and pyrolysis-free solvothermal process (*cf.* Fig. 1A).[26] The inexpensive and low-toxicity formamide (FA, as a solvent) can serve as a nitrogen source to *in situ* decorate CNTs while simultaneously generating Co–N species over the condensation reaction of FA.

[a] *CAS Key Laboratory of Urban Pollutant Conversion, Institute of Urban Environment (IUE), Chinese Academy of Sciences (CAS), No. 1799, Jimei Avenue, Xiamen 361021, China. E-mail: ymzheng@iue.ac.cn, mlfu@iue.ac.cn, mlfu@hqu.edu.cn*
[b] *University of Chinese Academy of Sciences (UCAS), No. 19(A), Yuquan Road, Shijingshan, Beijing 100049, China*
[c] *School of Civil and Environmental Engineering, Nanyang Technological University, 639798, Singapore*
[d] *Xiamen Key Laboratory of Municipal and Industrial Solid Waste Utilization and Pollution Control, College of Civil Engineering, Huaqiao University, Xiamen 361020, China*

† Electronic supplementary information (ESI) available. See DOI: 10.1039/d1cc05629h

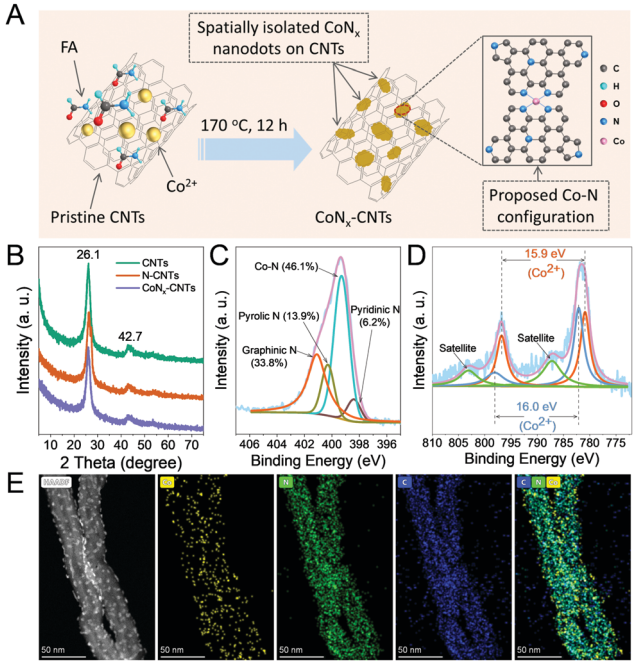

Fig. 1 Schematic illustration of the synthesis of CoN_x-CNTs and the proposed Co–N configuration (A). XRD patterns of CNTs, N-CNTs and CoN_x-CNTs (B). High-resolution N 1s XPS spectrum (C) and Co 2p XPS spectrum (D) of CoN_x-CNTs. HAADF-STEM image and EDS mapping of CoN_x-CNTs (E).

The resultant CoN_x-CNTs showed extraordinary activities in PMS activation under complicated water matrix conditions. Remarkably, the normalized pseudo-first-order kinetic rate constant to the dosage of catalyst reached 37.14 min^{-1} $(g\ L^{-1})^{-1}$, much higher than those for previously reported catalysts (even higher than those for some single-atom catalysts; *cf.* Table S1, ESI†).

The X-ray diffraction (XRD) patterns of CNTs, N-CNTs and CoNx-CNTs are shown in Fig. 1B. All the samples show two peaks at 26.1° and 42.7°, attributed to the {002} and {100} diffraction planes of CNTs (with a hexagonal graphite structure), respectively (JCPDS No. 41-1487). A peak at 27.6° appearing in the case of N-CNTs is probably due to the stacking of the conjugated structure in the {002} direction after N-doping. The peak at 27.6° disappeared after Co introduction, implying the reduced crystallinity of N-CNTs because of the coordination of Co with N species. The absence of metallic peaks suggests that the metal-containing species within CoN_x-CNTs are very small or amorphous, which agrees well with the TEM results (Fig. S1 (ESI†)). The full X-ray photoelectron spectroscopy (XPS) survey also confirms the successful N- and Co-doping on CNTs (Fig. S2A–C (ESI†)). The content of N within N-CNTs is 24.00 wt%, much higher than those of pyrolysis-based N-doped carbonaceous materials.[27,28] The nitrogen species within N-CNTs are pyridinic N (30.15%), pyrrolic N (43.87%), and graphitic N (25.97%) (Fig. S2D, ESI†), which can serve as anchoring sites for Co atoms. As expected, the content of N within CoN_x-CNTs was decreased to 12.49 wt% after Co doping (*cf.* Fig. S2C and D, ESI†). The decrease of pyridinic N and pyrrolic N species within CoN_x-CNTs is probably due to the coordination of Co and N atoms, while the peak appearing at 399.3 eV verifies the formation of Co–N (46.09%) within CoN_x-CNTs (Fig. 1C). The content of Co on the surface of CoN_x-CNTs is determined to be 2.06 wt% by XPS. The high-resolution Co 2p spectrum of XPS shows that the Co atoms exist in the oxidation form of Co^{2+} (Fig. 1D). The aberration-corrected high-angle annular dark-field scanning transmission electron microscopy (HAADF-STEM) image clearly demonstrates the spatially isolated CoN_x clusters on CNTs with quantum/nano-size (5–15 nm). The HAADF-STEM based energy-dispersive X-ray spectroscopy (EDS) reveals the homogeneous distribution of N and Co elements doped on the surface of CNTs (Fig. 1E).

The superior catalytic activity of CoN_x-CNTs is shown in Fig. 2A. In detail, the CoN_x-CNTs with an ultralow dosage (0.025 mg L^{-1}) can rapidly activate PMS (0.2 g L^{-1}) to remove > 98% of acid orange VII (AO7) within 5 min. The corresponding pseudo-first-order kinetic rate constant (k_{obs}) for AO7 removal can reach 0.93 min^{-1}. In contrast, N-CNTs, CoN_x and pristine CNTs are much inferior to CoN_x-CNTs in PMS activation/catalysis. The removal of AO7 by the PMS/CNT system is mainly attributed to the adsorption of CNTs within 10 min (Fig. S3A (ESI†)). Sole PMS can hardly oxidise AO7 within 10 min, and less than 5% of AO7 can be removed even if the time is prolonged to 120 min (refer to Fig. S3B (ESI†)). The catalytic activities of commercial nano-Co_3O_4 (cn-Co_3O_4, 100 nm), lab-synthesized β-MnO_2 and commercial nano-Fe_3O_4 (cn-Fe_3O_4, 20 nm) in PMS activation were also studied (Fig. S3B, ESI†). It is found that cn-Co_3O_4, β-MnO_2 and cn-Fe_3O_4 with a 20 times higher dosage of CoN_x-CNTs did not necessarily show desirable efficacy toward PMS activation. It will take 120 minutes to oxidise 90% of AO7 by the activated PMS with cn-Co_3O_4 and β-MnO_2. The normalized k_{obs} to the dosage of catalyst (denoted as k_d, min^{-1} $(g\ L^{-1})^{-1}$) was introduced to further better understand the catalytic activity of CoN_x-CNTs. As depicted in Fig. 2B, the k_d value of CoN_x-CNTs is 215.62, 37.98 and 12.73 times higher than those of pristine CNTs, CoN_x and N-CNTs, respectively. We attribute this to the synergistic effect of active N and Co species within CoN_x-CNTs. The k_d values for cn-Co_3O_4, β-MnO_2 and cn-Fe_3O_4 are 237.7, 74.6 and 679.4 times lower than that for CoN_x-CNTs, further confirming the superior catalytic activity of spatially isolated CoN_x

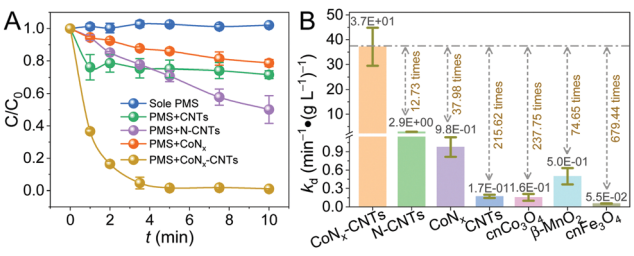

Fig. 2 (A) The AO7 degradation by sole PMS and the activated PMS with different catalysts under various conditions. (B) The comparison of the catalytic activities of CNTs, N-CNTs, CoN_x, CoN_x-CNTs, cn-Co_3O_4, β-MnO_2 and cn-Fe_3O_4 with respect to k_d for the degradation of AO7.

nanoclusters on CNTs. Moreover, the obtained k_d value for CoN_x-CNTs (37.14 min^{-1} $(g\ L^{-1})^{-1}$) is much higher than those for recently reported catalysts including single atom catalysts (*cf.* Table S1, ESI†).

The superiority of the $SO_4^{\bullet-}$- and $^{\bullet}OH$-free PMS/CoN_x-CNT system was further examined under different co-existing anions and initial solution pH values. It is obvious that the coexistence of environmentally important anions, such as Cl^-, NO_3^-, HCO_3^-, SO_4^{2-} and PO_4^{3-}, caused marginal impacts on the degradation of AO7 (Fig. 3A). More than 93% of AO7 can be degraded within 7.5 min with k_{obs} values of 0.73–1.1 min^{-1} (Table S2, ESI†). Moreover, CoN_x-CNTs can activate PMS to highly degrade AO7 in the initial pH range of 3–10.6 (Fig. 3B). The removal efficiencies and k_{obs} values for the degradation of AO7 in the wide initial pH range can be maintained at >97% and 0.65–0.93 min^{-1}, respectively (Table S2, ESI†). For the radical-oriented oxidation system, $SO_4^{\bullet-}$, $^{\bullet}OH$ and $O_2^{\bullet-}$ can react with inorganic anions (like HCO_3^- and PO_4^{3-}) to produce secondary radicals with low oxidation potential, which will inevitably suppress the oxidation degradation of pollutants.[11,29] Therefore, the negligible effects of Cl^-, HCO_3^- and PO_4^{3-} in this work, to some extent, verify that neither $SO_4^{\bullet-}$ nor $^{\bullet}OH$ was formed as the dominant oxidant for pollutant degradation.

To further reveal the potential of the PMS/CoN_x-CNT system in water decontamination, the degradation of other ROCs was tested (Fig. 3C and Table S3, ESI†). Above 97% of 2-chlorophenol (2-CP) was degraded in 5 min and the k_{obs} value reached 0.78 min^{-1}. Within 20 min, phenol, butyl paraben (BPB) and bisphenol A (BPA) were degraded by 94%, 98% and 97%, and the corresponding k_{obs} values are 0.35 min^{-1}, 0.32 min^{-1} and 0.30 min^{-1}, respectively (Table S2, ESI†). These findings imply that a broad spectrum of ROCs can be catalytically degraded by CoN_x-CNTs in the presence of PMS. Notably, when AO7 was introduced into real water samples to prepare simulated wastewaters, the degradation efficiency and kinetics of AO7 were barely affected (Fig. 3D). As tabulated in Table S2 (ESI†), the released Co ions from CoN_x-CNTs are lower than the Co discharge threshold (1 mg L^{-1}) guided by the environmental quality standard for surface water of China (GB3838-2002). This shows that CoN_x-CNTs are catalytically stable and robust in PMS activation under different environmental conditions. In summary, all these findings suggest the great potential of CoN_x-CNTs in wastewater decontamination under complex water matrix conditions.

The reactive species involved in the PMS/CoN_x-CNT system for AO7 degradation were examined by quenching tests (Fig. 4A). Ethanol (EtOH) is effective to quench $SO_4^{\bullet-}$ and $^{\bullet}OH$ (accordingly (1.6–7.7) × 10^7 M s^{-1} and 1.9 × 10^9 M s^{-1}), while *tert*-butyl alcohol (TBA) prefers to quench $^{\bullet}OH$ ((3.8–7.6) × 10^8 M s^{-1}); both EtOH and TBA are inert to other active $^1O_2$ and $O_2^{\bullet-}$ (<10^4 M s^{-1}).[30] Surprisingly, neither EtOH nor TBA can exert significant inhibition toward the degradation of AO7, indicating that $SO_4^{\bullet-}$ and $^{\bullet}OH$ are not the primary oxidation species for the pollutant degradation. In contrast, L-histidine (HD) and *p*-benzoquinone (BQ) remarkably suppressed the degradation of AO7. It should be noted that HD (only quenching $^1O_2$, 6.6 × 10^7 M s^{-1}) and BQ (quenching both $^1O_2$ and $O_2^{\bullet-}$, accordingly 3.8 × 10^7 M s^{-1} and ~ 10^9 M s^{-1}) have high second-order reaction rate constants with $SO_4^{\bullet-}$ and $^{\bullet}OH$ (10^8–10^9 M s^{-1}).[30] Since $SO_4^{\bullet-}$ and $^{\bullet}OH$ were not generated in the system, the inhibition of HD (inert to $O_2^{\bullet-}$, <1 M s^{-1}) indicates the formation of $^1O_2$. However, the inhibition caused by BQ did not necessarily mean that $O_2^{\bullet-}$ participated in the degradation of AO7 because of the reaction of $^1O_2$ with BQ. Previous work implies that HCO_3^- can quench $O_2^{\bullet-}$ effectively (5 × 10^8 M s^{-1}).[15] Based on the negligible effect of HCO_3^- on the degradation of AO7, we think that $O_2^{\bullet-}$ is not

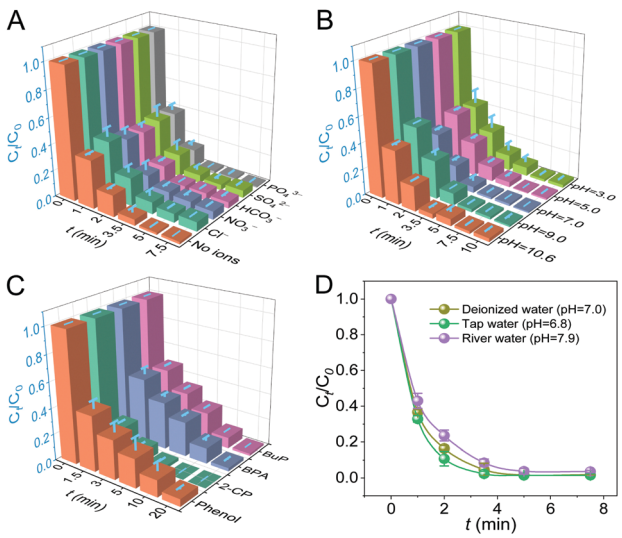

Fig. 3 The effects of common anions (A) and the initial solution pH (B) on the reactivity of CoN_x-CNTs toward PMS activation for degrading AO7. (C) The performance of the PMS/CoN_x-CNT system for degrading other ROCs. (D) The comparison of the degradation of AO7 in different water environmental conditions by the PMS/CoN_x-CNT system.

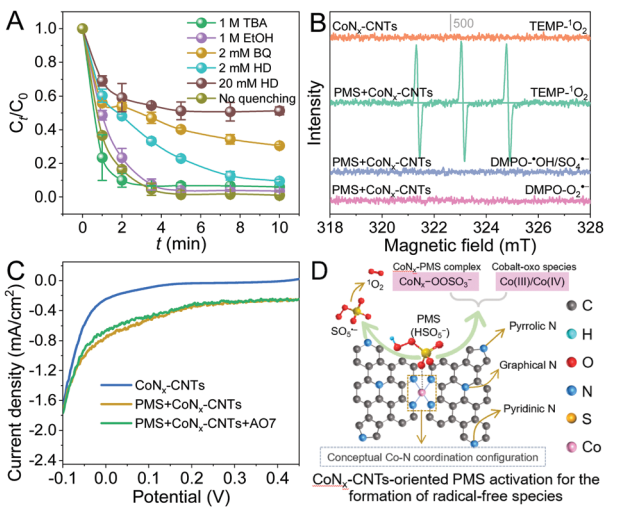

Fig. 4 (A) The effects of scavengers on AO7 degradation by the PMS/CoN_x-CNT system. (B) EPR spectra of DMPO-$^{\bullet}OH/SO_4^{\bullet-}$ adducts and TMEP-$^1O_2$ adducts in the PMS/CoN_x-CNT system (recorded at 1 min). (C) The LSV curves of the CoN_x-CNT related system. (D) The proposed activation mechanisms of PMS by CoN_x-CNTs and the formation of reactive species in the PMS/CoN_x-CNT system.

the primary reactive species for pollutant degradation by the PMS/CoN_x-CNT system. These results contradict the common knowledge that most of the Co-based oxides can activate PMS to produce $SO_4^{\bullet-}$ and/or $^{\bullet}OH$.[22,31]

Electron paramagnetic resonance (EPR) characterization studies further verify that no radicals, *i.e.*, $SO_4^{\bullet-}$, $^{\bullet}OH$ and $O_2^{\bullet-}$, were generated in the PMS/CoN_x-CNT system (Fig. 4B and Fig. S4A, B, ESI†). The remarkable signal of the TMEP-$^1O_2$ adduct suggests the formation of $^1O_2$ in the current system (Fig. 4B). For the linear sweep voltammetry (LSV) curves (Fig. 4C), the increased electron density of the CoN_x-CNT electrode in the PMS-containing Na_2SO_4 solution indicates the electron transfer from PMS to CoN_x-CNTs. However, the presence of AO7 did not increase the electron density of the CoN_x-CNT electrode in the PMS-containing Na_2SO_4 solution. This suggests that the CoN_x-CNTs after withdrawing electrons from PMS cannot directly donate electrons to AO7. We think that the electron transfer from PMS to CoN_x-CNTs (with special Co–N coordination configuration) induced the formation of $^1O_2$, the CoN_x-$OOSO_3^-$ complex and/or high-valence cobalt-oxo species (*cf.* Fig. 4D).[24] The incomplete inhibition of HD on the degradation of AO7 implies that $^1O_2$ was not the sole reactive species responsible for the oxidation degradation of AO7. We considered that, besides $^1O_2$, the CoN_x-$OOSO_3^-$ complex and/or high-valence cobalt-oxo species probably participated in the degradation of AO7 *via* oxygen atom transfer, which is also an effective non-radical pathway for the degradation of organic pollutants.[32,33] The undesirable reusability of CoN_x-CNTs suggests the necessity of exploring their regeneration methods and even reconstructing their catalytic sites (Fig. S4C, ESI†). The changeable toxicity of the degradation products of AO7 merits an in-depth study of critically assessing the health and ecological risks of radical-free and selective oxidation of contaminants (*cf.* Fig. S5 and Table S4, ESI†).[34]

In summary, a cost-effective strategy has been established for developing spatially isolated CoN_x quantum dots on CNTs *via* a simple formamide condensation reaction. It is found that pyrolysis-free CoN_x-CNTs are robust in PMS activation, even superior to some newly reported single-atom catalysts. More interestingly, the radical-free pathways for degrading ROCs enabled by CoN_x-CNTs show excellent anti-interference capacity toward complicated water chemistry constitutes. Through this work, whether in the community of chemistry/materials or in the field of environmental remediation, we hope to initiate more research interest in developing facile, mild and cost-effective ways to construct multifunctional catalysts with their active sites fully exposed at the quantum-/atom-sized scale.

The authors acknowledge the National Natural Science Foundation of China (Grant No. 51808524, 51778598 and 51978639) and the Natural Science Foundation of Fujian Province (Grant No. 2020J01120).

Conflicts of interest

There are no conflicts to declare.

Notes and references

1 B. C. Hodges, E. L. Cates and J. Kim, *Nat. Nanotechnol.*, 2018, **13**, 642–650.
2 J. Ma, D. Minakata, K. O'Shea, L. Bai, D. D. Dionysiou, R. Spinney, R. Xiao and Z. Wei, *Water Res.*, 2021, **190**, 116746.
3 M. Hayyan, M. A. Hashim and I. M. AlNashef, *Chem. Rev.*, 2016, **116**, 3029–3085.
4 Z. Zhou, J. Song, L. Nie and X. Chen, *Chem. Soc. Rev.*, 2016, **45**, 6597–6626.
5 Y. Tan, Z. Chai, B. Wang, S. Tian, X. Deng, Z. Bai, L. Chen, S. Shen, J. Guo, M. Cai, C. Au and S. Yin, *ACS Catal.*, 2021, **11**, 2492–2503.
6 J. B. Pan, S. Shen, L. Chen, C. T. Au and S. F. Yin, *Adv. Funct. Mater.*, 2021, **31**, 2104269.
7 J. B. Pan, B. H. Wang, J. B. Wang, H. Z. Ding, W. Zhou, X. Liu, J. R. Zhang, S. Shen, J. K. Guo, L. Chen, C. T. Au, L. L. Jiang and S. F. Yin, *Angew. Chem., Int. Ed.*, 2021, **60**, 1433–1440.
8 J. Lee, U. von Gunten and J. Kim, *Environ. Sci. Technol.*, 2020, **54**, 3064–3081.
9 W. Li, X. Chu, S. He, X. Wang and C. Wang, *Environ. Sci.: Nano*, 2020, **7**, 2654–2668.
10 H. Li, C. Shan, W. Li and B. Pan, *Water Res.*, 2018, **147**, 233–241.
11 J. E. Yang, Y. Lin, H. Peng, B. Yuan, D. D. Dionysiou, X. Huang, D. Zhang and M. Fu, *Appl. Catal., B*, 2020, **268**, 118549.
12 N. Jiang, H. Xu, L. Wang, J. Jiang and T. Zhang, *Environ. Sci. Technol.*, 2020, **54**, 14057–14065.
13 J. Ji, Q. Yan, P. Yin, S. Mine, M. Matsuoka and M. Xing, *Angew. Chem., Int. Ed.*, 2021, **60**, 2903–2908.
14 J. Peng, P. Zhou, H. Zhou, W. Liu, H. Zhang, C. Zhou, L. Lai, Z. Ao, S. Su and B. Lai, *Environ. Sci. Technol.*, 2021, **55**, 9189–9198.
15 A. Jawad, K. Zhan, H. Wang, A. Shahzad, Z. Zeng, J. Wang, X. Zhou, H. Ullah, Z. Chen and Z. Chen, *Environ. Sci. Technol.*, 2020, **54**, 2476–2488.
16 W. Peng, Y. Dong, Y. Fu, L. Wang, Q. Li, Y. Liu, Q. Fan and Z. Wang, *Chem. Eng. J.*, 2021, **421**, 127818.
17 M. Babucci, A. Guntida and B. C. Gates, *Chem. Rev.*, 2020, **120**, 11956–11985.
18 Z. Li, S. Ji, Y. Liu, X. Cao, S. Tian, Y. Chen, Z. Niu and Y. Li, *Chem. Rev.*, 2020, **120**, 623–682.
19 Y. Shang, X. Xu, B. Gao, S. Wang and X. Duan, *Chem. Soc. Rev.*, 2021, **50**, 5281–5322.
20 W. Li, X. Chu, F. Wang, Y. Dang, X. Liu, X. Wang and C. Wang, *Appl. Catal., B*, 2021, **288**, 120034.
21 L. Su, P. Wang, X. Ma, J. Wang and S. Zhan, *Angew. Chem., Int. Ed.*, 2021, **60**, 21261–21266.
22 Z. Y. Guo, C. X. Li, M. Gao, X. Han, Y. J. Zhang, W. J. Zhang and W. W. Li, *Angew. Chem., Int. Ed.*, 2021, **60**, 274–280.
23 L. S. Zhang, X. H. Jiang, Z. A. Zhong, L. Tian, Q. Sun, Y. T. Cui, X. Lu, J. P. Zou and S. L. Luo, *Angew. Chem., Int. Ed.*, 2021, **60**, 21751–21755.
24 X. Mi, P. Wang, S. Xu, L. Su, H. Zhong, H. Wang, Y. Li and S. Zhan, *Angew. Chem., Int. Ed.*, 2021, **60**, 4588–4593.
25 Z. Yang, J. Qian, A. Yu and B. Pan, *Proc. Natl. Acad. Sci. U. S. A.*, 2019, **116**, 6659–6664.
26 G. Zhang, Y. Jia, C. Zhang, X. Xiong, K. Sun, R. Chen, W. Chen, Y. Kuang, L. Zheng, H. Tang, W. Liu, J. Liu, X. Sun, W. Lin and H. Dai, *Energy Environ. Sci.*, 2019, **12**, 1317–1325.
27 X. Duan, K. O'Donnell, H. Sun, Y. Wang and S. Wang, *Small*, 2015, **11**, 3036–3044.
28 J. Miao, W. Geng, P. J. J. Alvarez and M. Long, *Environ. Sci. Technol.*, 2020, **54**, 8473–8481.
29 M. Zhu, J. E. Yang, X. Duan, D. Zhang, S. Wang, B. Yuan and M. Fu, *Chem. Eng. J.*, 2020, **397**, 125339.
30 J. E. Yang, M. Zhu, X. Duan, S. Wang, B. Yuan and M. Fu, *Appl. Catal., B*, 2021, **297**, 120460.
31 Y. Wang, Z. Chi, C. Chen, C. Su, D. Liu, Y. Liu, X. Duan and S. Wang, *Appl. Catal., B*, 2020, **272**, 118972.
32 Y. Zong, X. Guan, J. Xu, Y. Feng, Y. Mao, L. Xu, H. Chu and D. Wu, *Environ. Sci. Technol.*, 2020, **54**, 16231–16239.
33 Y. Zhao, C. Deng, D. Tang, L. Ding, Y. Zhang, H. Sheng, H. Ji, W. Song, W. Ma, C. Chen and J. Zhao, *Nat. Catal.*, 2021, **4**, 684–691.
34 Z. Yang, J. Qian, C. Shan, H. Li, Y. Yin and B. Pan, *Environ. Sci. Technol.*, 2021, **55**, 14494–14514.

